Talanta 205 (2019) 120091

Contents lists available at ScienceDirect

Talanta

journal homepage: www.elsevier.com/locate/talanta

Nitrogen-doped porous carbon-based fluorescence sensor for the detection of ZIKV RNA sequences: fluorescence image analysis

Jie Li[a], Ke Yang[b,*], Zheng Wu[a], Xuede Li[a], Qingyun Duan[a]

[a] School of Resources and Environment, Anhui Agricultural University, Hefei, Anhui, PR China
[b] Institute of Applied Technology, Hefei Institutes of Physical Science, Chinese Academy of Sciences, Hefei, Anhui, PR China

ARTICLE INFO

Keywords:
Nitrogen-doped porous carbon
ZIKV RNA sequences
Fluorescence quenching and recovery
CCD-Based imaging platform

ABSTRACT

Many studies have demonstrated that metal-organic frameworks (MOFs) are universal fluorescence quenchers for DNA/RNA detection. Nevertheless, the structural stability of many MOFs is relatively weak, which limits their practical applications. Thus, it remains a great interest to develop constitutionally stable nano biosensor suitable for application in the complex environment. Herein, a new angle of nitrogen-doped porous carbon (NPC) obtained from MOFs-based precursors by virtue of a simple method was applied as a nano biosensor for the fluorescence detection of Zika virus (ZIKV) RNA sequences. The fluorescence signal capturing was carried out by using a charge-coupled device (CCD)-based imaging system. The NPC could adsorb TAMRA-tagged ZIKV RNA probe (P-DNA) to form P-DNA@NPC complex accompanied by substantial fluorescence quenching. Upon adding the complementary target RNA (T-RNA), the P-DNA could release from NPC by forming a double-stranded hybrid and induce the fluorescence recovery. The P-DNA@NPC complex was valid and reliable for ZIKV RNA sequences assay with a limit of detection (LoD) at 0.23 nM, which is superior to many of the previously reported fluorescent DNA sensors. Moreover, it could distinguish mismatched RNA and was effective in detecting ZIKV RNA sequences spiked in the human saliva sample. We envision that this study would offer an interesting new angle on the potential integrating application of carbon nanomaterials and CCD-based fluorescence imaging platform in the field of nucleic acid assay.

1. Introduction

In recent years, Zika virus (ZIKV) has become a significant cause of public safety, because it is closely related to a variety of neurological diseases, such as Guillain Barré syndrome in adults and microcephaly in newborns [1,2]. The diagnosis of ZIKV is not easy because it is a kind of latency disease and the infected person shows either no or only common symptoms such as retro-orbital pain, arthralgia, and fever [3–5]. Nucleic acid test (NAT) and immunoassay are recommended by the US Centers for Disease Control and Prevention for examining those patients who show the symptoms with possible ZIKV infection [6]. While loop-mediated isothermal amplification (LAMP) and polymerase chain reaction (PCR) are often used as a NAT, they both have limitations such as high costs and/or risk of false positive results due to carryover contamination [7–9]. Moreover, ZIKV is contagious during the incubation period and is difficult to be determined by immunological analysis techniques [10]. Therefore, there is a great interest to develop other diagnostic methods that are not replace LAMP and PCR, but rather supplement them as effective screening tools for ZIKV detection.

At present, numerous nanomaterials-based fluorescence quenchers have been employed for DNA/RNA detection. These nanomaterials, such as gold nanoparticles [11], MoS_2 nanosheet [12], carbon nanotubes [13], graphene oxide [14], iron oxide nanoparticles [15], and conductive polymers such as polypyrrole nanospheres [16] and polyaniline nanofibers [17], etc., mainly adsorbed the fluorophore-labeled DNA probe through specific interaction mechanism, thus leading to the fluorescence quenching. The recovery of fluorescence would only be achieved by adding a target DNA complementary to the DNA probe. However, it would be convenient to simplify the corresponding operational procedures, and a suitable method of achieving this type of test, is by preloading the nanomaterials and DNA probe of interest in the containers (e.g. PCR tubes) that could be stored for later use, allowing more convenient for the creation of nanomaterials@DNA probe complex. In other words, the nanomaterials could be conveniently interacted with the probe DNA and then used as a test system, which would reduce the time required to complete a test. Thus, nanomaterials with long-term stability is crucial for achieving this type of

* Corresponding author.
E-mail address: keyang@rntek.cas.cn (K. Yang).

https://doi.org/10.1016/j.talanta.2019.06.091
Received 6 April 2019; Received in revised form 21 June 2019; Accepted 26 June 2019
Available online 29 June 2019
0039-9140/

performance.

Metal-organic frameworks (MOFs) are an emerging class of porous materials, comprising of organic linkers and metal ions/clusters [18,19]. In the development of new sensing platforms, MOFs have attracted more and more attention in the field of nucleic acid assay due to their excellent quenching ability toward the fluorescence-labeled single-stranded DNA (ssDNA) [20–24]. However, the structural stability of MOFs is relatively weak in the solution containing various ions (e.g. Na^+, Mg^{2+}, Cl^-), or under a wide range of conditions, such as pH values, thus limiting their practical applications [22,25–27]. In the past few years, MOFs have been widely exploited as sacrificial templates to fabricate various kinds of porous carbons, which benefits from their high surface areas and porous structure [28]. Due to the unique properties (e.g., low-cost, good conductivity, and chemical stability), MOFs-derived porous carbons show great promise in the application of energy storage, catalysis and environment [29–32]. MOFs-derived carbons have also been available for biomolecular detection due to their excellent electrochemical properties. For instance, carbon materials were claimed to be effective sensing platforms for nucleic acid detection due to their properties for selectively adsorbtion and quenching fluorescence-labeled ssDNA [15,33–35]. However, the preparation of most of these carbon materials is tedious with low production rate. In addition, to the best of our knowledge, only one study from Tan et al. reported MOFs-derived porous carbon for DNA detection [25]. They found that the carbon materials derived from thermolysis of iron-containing MOFs (MIL-88A) exhibited excellent selectivity to HIV with a LoD of 1 nM. Accordingly, sensing platforms based on MOFs-derived carbon for the detection of viral nucleic acid, especially ZIKV are limited. The mechanism behind the MOF-derived carbon for the nucleic acid assay also need further investigation. Besides, the demonstration of the practical application of MOFs-derived carbon for detecting the nucleic acid sequences spiked in the real samples is a crucial step to study the reliability and applicability of the proposed detection method. Therefore, there is an urgent need to develop novel highly sensitive carbon nanosensors for the detection of ZIKV RNA sequences, even in real samples.

Herein, we aimed to 1) obtain nitrogen-doped porous carbon (NPC) by using MOFs-based composites as precursors and validate its feasibility for ZIKV RNA sequences detection with a CCD-based imaging system; 2) carry out a serial studies to evaluate the sensitivity and specificity of the NPC for ZIKV RNA sequences assay; and 3) detect the ZIKV RNA sequences spiked in human saliva samples to evaluate the potential applications of NPC in real samples in the future.

2. Experimental section

2.1. Design of ZIKV specific DNA probe

ZIKV is a single-stranded RNA virus composed of 10,794 bases that encode seven non-structural proteins (NS1, 2A, 2aB, 3, 4A, 4B, 5) and three structural proteins (Capsid, precursor-Membrane, Envelope) [36]. The NS5 protein is the largest ZIKV protein, and its short C is closely related to RNA-dependent RNA polymerase activity [37]. Thus, the NS5 was chosen as the specific target sequence. The method for NS5 sequence construction was as follows: 1) Twenty kindss of known ZIKV were chosen and their corresponding genomic sequences were downloaded from the National Center for Biotechnology Information (NCBI); 2) DNA MAN (sequence analysis software) was used to compare the different genomic sequences and screen the specific NS5 sequence of ZIKV as the target fragment; and 3) all oligonucleotides were synthesized by Shanghai Sangon Biological Engineering Technology & Services Co., Ltd. (China). The P-DNA and the corresponding mutation sequences are as follows (mismatch underlined).

Probe DNA for ZIKV (P-DNA):

5′-TAMRA-ACATGGACTACCTATCCACCCAAGT-3′

Complementary target RNA for ZIKV (T-RNA, T0):

5′-ACUUGGGUGGAUAGGUAGUCCAUGU-3′

Single-base mismatched target RNA for ZIKV (T1):

5′-ACUUGGGUGGAU**G**GGUAGUCCAUGU-3′

Double-base mismatched target RNA for ZIKV (T2):

5′-ACUUGGGUGGAU**G**G**C**UAGUCCAUGU-3′

Non-complementary RNA sequences (T3):

5′-AGUCUGUAGUCAUUAGCGUCGCG-3′

P-DNA was TAMRA-tagged at 5′-terminal, and thus the hybridization of P-DNA and T-RNA can be monitored by measuring the change of fluorescence intensity. All sequences were dissolved in 20 μL of 20 mM Tris-HCl buffer solution (pH = 7.42, containing 100 mM NaCl, 5 mM KCl and 5 mM $MgCl_2$) at a concentration of 20 nM and stored in the PCR tubes at 4 °C for later use. The concentrations of P-DNA were chosen based on a preliminary investigation that showed the fluorescence quenching and recovery results were entirely satisfactory (see section 3.3). Detailed protocol about the preparation of Tris-HCl buffer solution is provided in the Supplementary Material.

2.2. CCD-based imaging system

The advantages of fluorescence imaging method are that it can effectively overcome the interference of background fluorescence and provide an attractive view for this task [38]. The fluorescence detection system is illustrated in Fig. 1A. The mechanical parts were first designed using Solidworks software and then fabricated using Computer Numerical Control (CNC) center before creating the assembly (Fig. 1B). The central principle of the optical path design was to collect enough light from the LED (CBT90, Luminus Devices, Inc., China) into the optical rod and enlarge to achieve uniform excitation in a 40 mm × 40 mm area. The light source from the LED was converted to 560 nm beam by the optical rod and excitation filter (Center wavelength 550, bandwidth 15 nm, Povet Technology Co., Ltd., China), then reflected by a dichroic beam splitter (Reflection 550 nm, transmission 590 nm, Siberia Technology Co., Ltd., China), and shined onto the PCR tubes. The excited fluorescence signal from the PCR tubes was captured by the CCD camera (MC20, Mingmei Photoelectric Technology Co., Ltd., Guangzhou, China) equipped with an emission filter (Enter wavelength 590, bandwidth 10 nm, Povet Technology Co., Ltd., China). The excitation light can be replaced conveniently according to the requirements for different fluorescent probes.

2.3. Fluorescent detection

The principle for detecting the ZIKV RNA sequences by the NPC is depicted in Scheme 1. For the fluorescence quenching experiment, 20 μL of NPC (20 μg/mL) was placed to interact with 20 μL of 20 nM TAMRA-labeled P-DNA in PCR tubes and stirred in a constant temperature mixer (Maofeng Instrument Co., Ltd., Hangzhou, China) at 800 rpm for 40 min at 60 °C to form P-DNA@NPC complex (Scheme 1, Fig. 1C). Then, P-DNA@NPC complex was incubated with 20 μL of T-RNA at different concentrations for another 80 min at room temperature (~25 °C) to perform the hybridizations until the saturation of fluorescence recovery (Scheme 1, Fig. 1C). Fluorescence quenching and recovery were monitored by using the CCD-based image system (Fig. 1A and B). Each experiment was repeated for three times. For each experiment, there are two PCR reaction tubes (Hole 1 and Hole 2) to make parallel (Fig. 1C). Data analysis was performed by using ImageJ (NIH, version 1.44) and its command of “Analyze/Measure/“. The

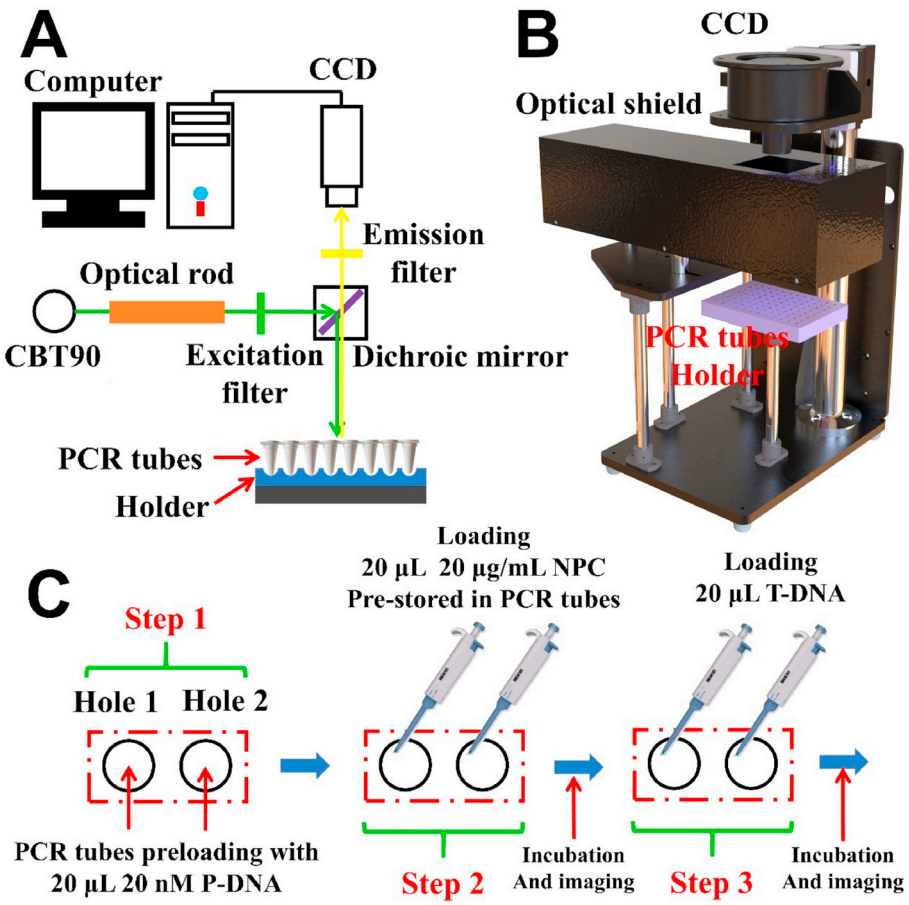

Fig. 1. An illustration of the fluorescence imaging system. (A) The optical configuration: a light source, an excitation light filter, a dichroic mirror, an emission filter, a CCD, a computer, a group of polymerase chain reaction tube; (B) A real picture of the assembled imaging platform; (C) Sample loading process. Step 1: take out the PCR tubes preloading with 20 µL 20 nM P-DNA; Step 2: loading 20 µL 20 nM P-DNA, incubation and imaging; Step 3: loading 20 µL T-DNA at the concentration of interest, incubation and imaging.

measurements were exported to Excel for further plotting. The quenching efficiency was calculated as QE = (1 − FM/F0) × 100%, wherein FM and F0 are the fluorescence intensities with and without NPC, respectively. The fluorescence recovery efficiency was calculated as RE = (FM-FT)/FM × 100%, wherein FM and FT are the fluorescence intensities with and without the T-RNA, respectively.

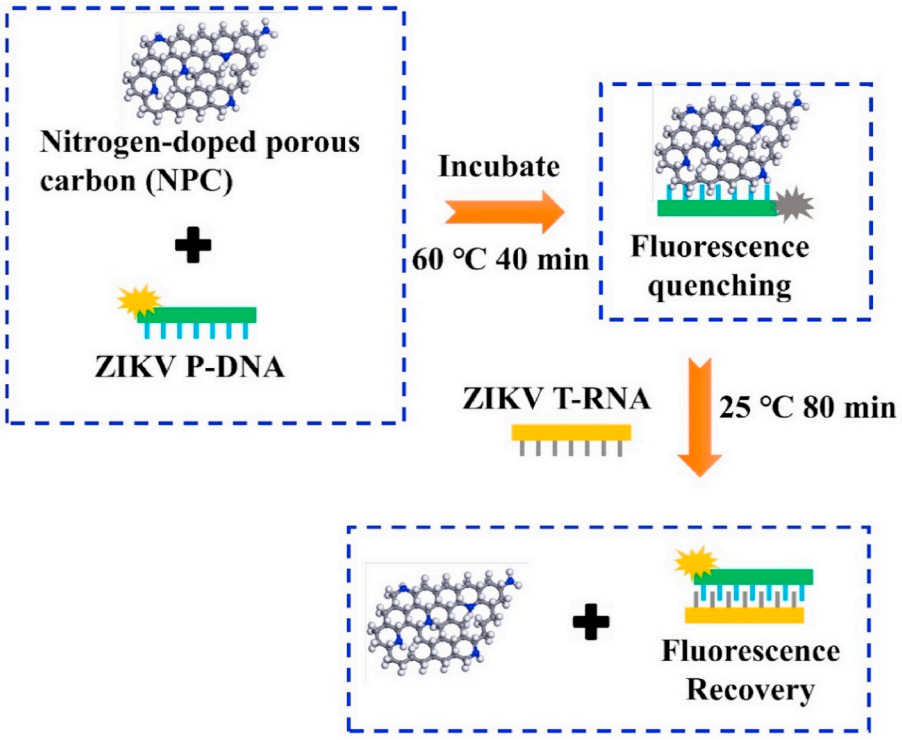

Scheme 1. Schematic illustration of the principle of detecting ZIKV with NPC as a sensing platform.

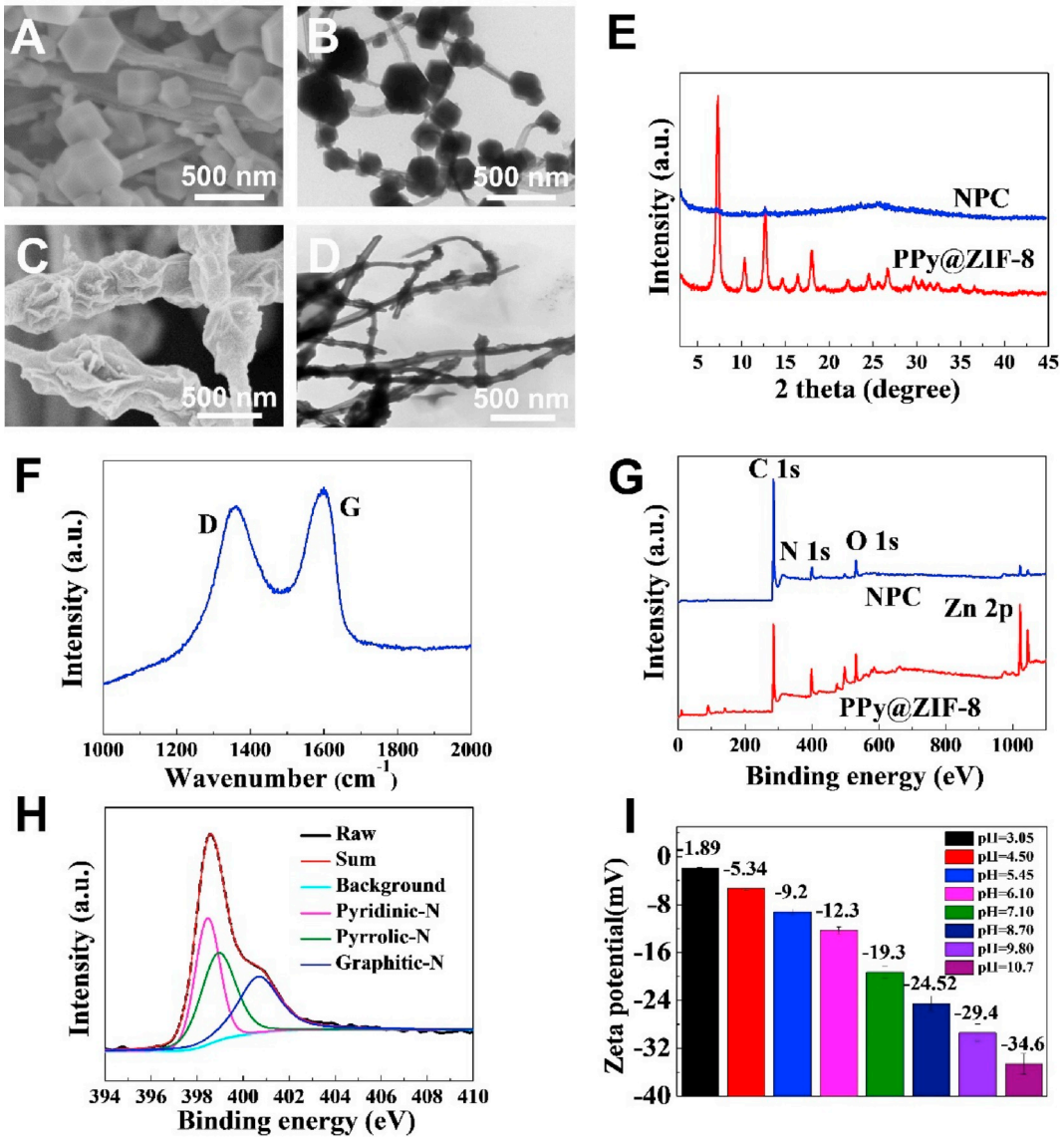

Fig. 2. Characterization results of NPC adsorbents. SEM image of PPy@ZIF-8 (A); TEM image of PPy@ZIF-8 (B); SEM image of NPC (C); TEM image of NPC (D); Comparison of the XRD patterns (E); Raman pattern of NPC (F); XPS survey scan spectra (G); N 1s spectra of NPC (H); and Zeta potentials of NPC in different solution pH (I).

2.4. Biological sample analysis

Human saliva sample was used to investigate the feasibility of the P-DNA@NPC system for DNA recognition in more realistic complex media. The collected saliva sample was first diluted 100 × in the Tris-HCl buffer solution. Then using the standard dilution method, different concentrations (10, 100 and 600 nM) of T-RNA were prepared by diluting the saliva sample. Afterwards, the solutions (diluted saliva sample and Tris-HCl) with or without T-RNA were tested using the P-DNA@NPC system.

3. Results and discussion

3.1. Characterization of NPC

Detailed information about the synthesis and characterization methods of the NPC are shown in the Supplementary Material. The scanning electron microscope (SEM) and transmission electron microscope (TEM) images of PPy@ZIF-8 composites and NPC are shown in Fig. 2(A-D). The as-prepared PPy@ZIF-8 precursor shows a net structure. After carbonization, the framework of ZIF-8 particles is slightly collapsed. Only one broad peak located at around 26° presents on the X-Ray Diffraction (XRD) pattern of the obtained NPC, which is the representative carbon diffractions, indicating the thorough carbonization of the PPy@ZIF-8 templates (Fig. 2E). Raman technique was further exploited to determine the carbonization degree of NPC (Fig. 2F). In its Raman spectrum, two prominent peaks at ~1350 (D band) and ~1590 cm^{-1} (G band) are observed, which are the signatures for the in-plane vibration of the graphitic sp^2 carbons and the presence of structural defects, respectively. The intensity ratio of the D and G band was calculated to be 1.30. X-ray photoelectron spectroscopy (XPS) measurements were conducted to understand the element information of the obtained NPC further. Fig. 2G illustrates that NPC shows an obvious C 1s peak centered at ca. 285 eV, an N 1s peak centered at ca. 400 eV and an O 1s peak centered at ca. 540 eV. No peaks assigned to Zn 2p was detected, disclosing the complete removal of Zn residues via acid treatment. Additionally, the high resolution of N 1s signal can be deconvoluted into three peaks containing pyridinic-N at ~398.7 eV, pyrrolic-N at ~400 eV and graphitic-N at ~400.7 eV (Fig. 2H). The zeta potential of NPC in different pH values shows a

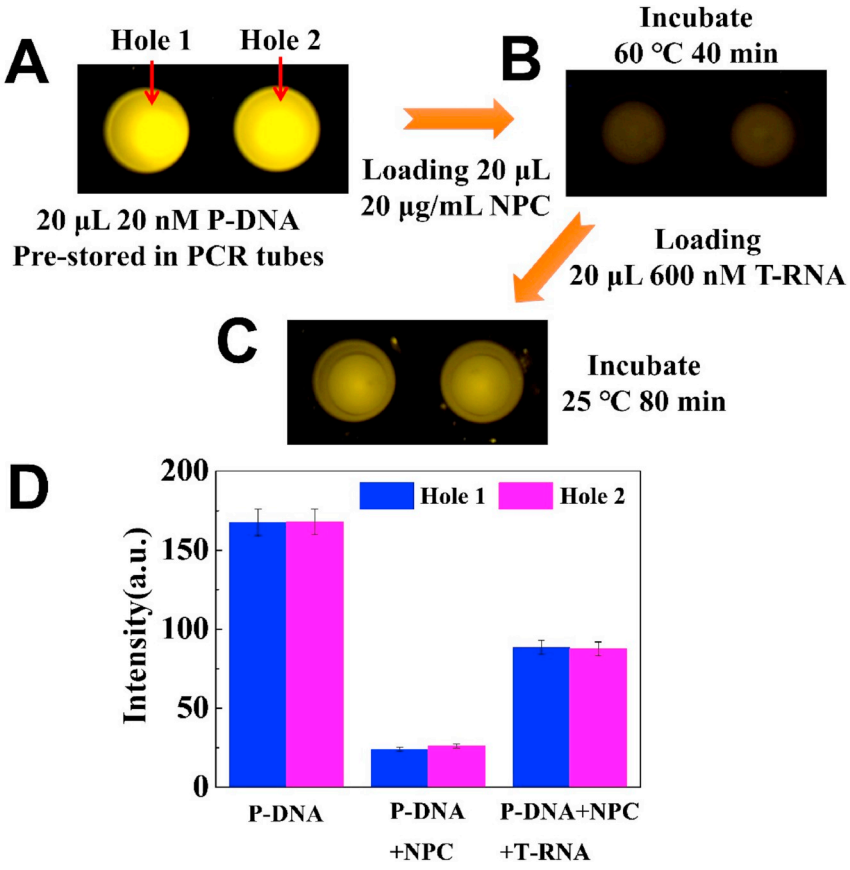

Fig. 3. Fluorescence image and intensity in different conditions when testing NPC. (A) 20 μL 20 nM P-DNA pre-stored in PCR tubes; (B) 20 μL 20 nM P-DNA + 20 μL 20 μg/mL NPC after incubation at 60 °C for 40 min; (C) 20 μL 20 nM P-DNA + 20 μL 20 μg/mL NPC + T-RNA (600 nM) after incubation at 85 °C for 80 min; (D) Comparation of the fluorescence intensity in different conditions.

negatively charged surface of NPC (Fig. 2I). The above observations confirm that the NPC derived from PPy@ZIF-8 composites has been successfully fabricated.

3.2. Verification of NPC-based ZIKV RNA sequences sensing

The procedure for the detection of ZIKV RNA sequences includes the adsorption of fluorescence-tagged P-DNA on the surface of NPC and subsequently the quenching of the fluorescence (Scheme 1). Then, T-RNA is added and in contact with the P-DNA@NPC. The specific hybridization of P-DNA and T-RNA results in the release of P-DNA from the NPC and fluorescence recovery [39–41]. The subsequent experiments validated this hypothesis. As shown in Fig. 3, we present the fluorescence images of the P-DNA under different conditions. It is apparent that the P-DNA showed strong fluorescence emission due to the coupling of TAMRA with the probe (Fig. 3A, D). While the fluorescence intensity decreases strongly (quenching efficiency, QE = 85%) after a 40 min interaction with NPC (Fig. 3B, D). The above experimental results showed the strong adsorption of P-DNA on the NPC. By contrast, after a double-stranded DNA (dsDNA) hybridized from P-DNA and T-RNA contact with the NPC, only a slight change in fluorescence intensity is observed (Fig. S1). This could be easily understood if one takes into account the affinities difference between the ssDNA and dsDNA towards the NPC, that is the affinity of the dsDNA towards the NPC is much weaker than the ssDNA [42]. After the P-DNA firmly immobilized, a solution of the T-RNA was loaded into the P-DNA@NPC solution. Then, a recovery response (recovery efficiency, RE = 251%) was indeed found after 80 min (Fig. 3C and D). The fluorescence recovery can be easily understood if one considers that the hybridization of P-DNA with T-RNA disturbed the interaction of P-DNA with NPC. When the same experiment was repeated by using PPy@ZIF-8 composite, it was found that the fluorescence recovery value after adding the T-RNA were not satisfactory (Fig. S2). In addition, it is also worth noting that the fluorescence of P-DNA is nearly not affected by the T-RNA without NPC and the PPy/ZIF-8/PPy@ZIF-8 composite/NPC themselves show no fluorescence contribution in the investigated wavelength range (data no shown). This initial experiment confirmed that the NPC could serve as a potential quencher for the detection of ZIKV RNA.

3.3. Adsorption, fluorescence quenching and recovery mechanism of NPC

In this study, it is reasonable to deduce that NPC can adsorb P-DNA through π–π interaction, hydrogen bonding, and electrostatic attraction to form P-DNA@NPC complex, and then quench the fluorescence of TAMRA through fluorescence resonance energy transfer (FRET) [43,44]. The main causes are as follows:1) Previous studies have demonstrated that there is a π-π interaction between ssDNA and various carbon materials, such as carbon nanoparticles [45], graphene oxide (GO) [46,47], and carbon nanotubes (CNTs) [48]. Thus, π-π interaction should also exist between the ssDNA and graphitized NPC (Fig. 2F); 2) NPC possesses abundant N atoms (Fig. 2H), which could serve as the H-bonding acceptor. Meanwhile, P-DNA possesses numerous –OH group which could also act as the H-bonding acceptor and donor. Thus, hydrogen bonding also participated in the adsorption of ssDNA by NPC; 3) the zeta potential of the NPC spiked in Tris-HCl buffer solution was −19.30 mV (Fig. 2I). In this case, there should be an electrostatic attraction between the NPC and TAMRA-tagged T-RNA with positively charged backbone [44]; and 4) the adsorption spectrum of NPC exhibits a wide window (λ ≈ 200–800 nm), suggesting that there is spectral overlap with the emission wavelength of TAMRA (Fig. S3). Thus, FRET should play a key role in quenching the fluorescence of P-DNA by NPC. Upon adding the T-RNA, P-DNA@T-RNA hybrid was formed and the bases would be hidden in the double-stranded structure, which resulted in a change in the conformation of the P-DNA, and the bases available for the bind with NPC were decreased. At the same time, the formed P-

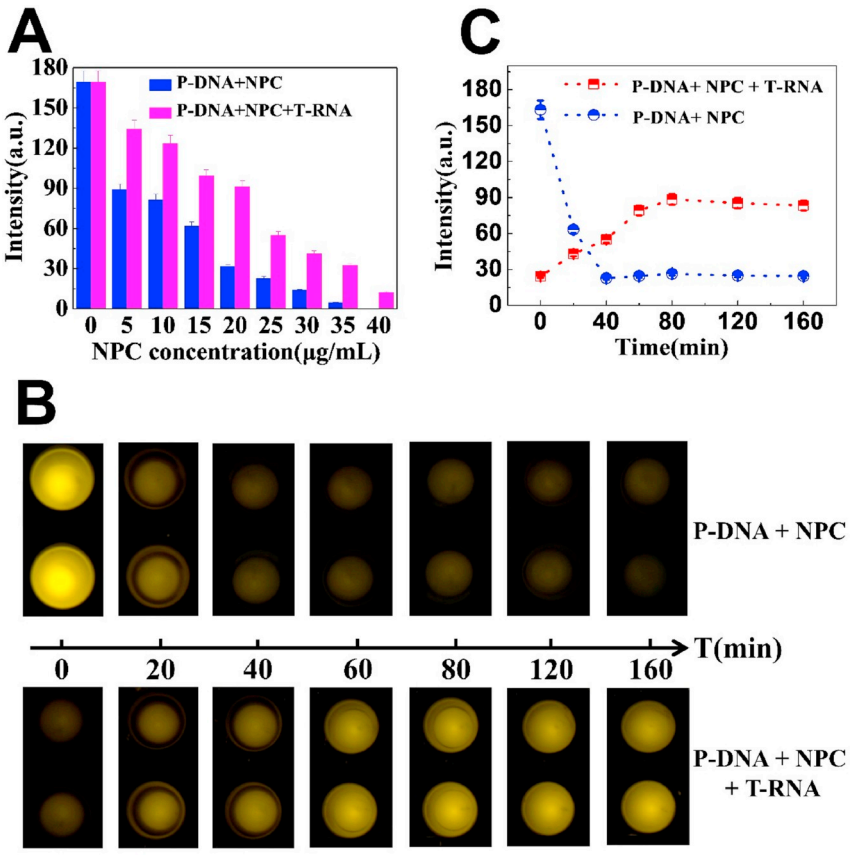

Fig. 4. (A) Fluorescence intensity of P-DNA (20 nM) + NPC and P-DNA (20 nM) + NPC + T-RNA (600 nM) in the presence of different NPC dosage (0, 5, 10, 15, 20, 25, 30, 35 40 μg/mL). (B) Fluorescence quenching images of P-DNA (20 nM) + NPC (20 μg/mL) and fluorescence recovery images of P-DNA (20 nM) + NPC (20 μg/mL) + T-RNA (600 nM) as a function of incubation time. (C) Fluorescence intensity of P-DNA (20 nM) + NPC (20 μg/mL) and fluorescence intensity of P-DNA (20 nM) + NPC (20 μg/mL) + T-RNA (600 nM) as a function of incubation time.

DNA@T-RNA hybrid will be far away from the NPC due to the reduced adsorption affinity caused by the rigidity of double-chain structure [41]. Therefore, the fluorescence of dye molecules was recovered.

3.4. Experimental conditions optimization

To establish the best experimental conditions of using the NPC for ZIKV RNA assay, various experimental parameters were explored, such as 1) the dosage of NPC, 2) the time allowed to quench the TAMRA-labeled P-DNA, and 3) the time suitable for the fluorescence recovery. To this end, we first examined the quenching and recovery of the fluorescence at different doses of NPC. As shown in Fig. 4A, the increase of NPC will lead to higher QE but lower RE. This is due to that more NPC can cause more efficient adsorption of the P-DNA. At the same time, the superfluous NPC would adsorb the T-RNA during the hybridization process, which results in the decreased hybridization and fluorescence recovery. In the following experiments, an optimal concentration of 20 μg/mL of NPC was used to obtain the best sensitivity.

In Fig. 4B and C, we present the kinetic progress of the adsorption of P-DNA on the NPC and show how the fluorescence intensity increases as the hybridization of P-DNA with T-RNA. The fluorescence images become darker as the incubation time increased (Fig. 4B). It takes 40 min before reaching equilibrium (Fig. 4C). When in the presence of the T-RNA, the image slowly lighted up as the increase of incubation time (Fig. 4B), because more adsorbed P-DNA released from the NPC. The fluorescence intensity did not exhibit further increase when the incubation time exceeded 80 min, indicating that the system reached equilibrium between P-DNA@NPC complex and the P-DNA@T-RNA hybrid (Fig. 4C). Therefore, in this study, 40 min and 80 min were selected as the optimal incubation time for the adsorption and detachment. Fig. S4A illustrates that NPC possesses hysteresis loops due to capillary condensation within pores, denoting its mesoporous structures. Moreover, the steep adsorption isotherm appeared at $P/P_0 < 0.1$ denotes the existence of micropores. Fig. S4B reveals that the obtained NPC was hierarchically porous with both micropores and mesopores, which is beneficial for the adsorption of base sequences. Therefore, the long recovery time could partly due to the adsorption of P-DNA by the pores of NPC by its non-TAMRA end.

3.5. Sensitivity analysis

In order to evaluate the sensing range and LoD of the NPC, a detailed fluorescence recovery experiment was implemented using different concentrations of T-RNA. The fluorescence intensity in the 1–1000 nM range of T-RNA is shown in Fig. 5A. When NPC@P-DNA was exposed to the increased concentrations of T-RNA, more P-DNA was released from the surface of NPC (Fig. 5A). Then, the fluorescence intensity increased due to a large number of P-DNA@T-RNA heterozygotes formed. The recovery fluorescence intensity reached saturation at 600 nM of T-RNA. A linear relationship between the fluorescence intensity (Y) and the concentration of T-RNA (X) was found with a correlation coefficient (R^2) at 0.983, in the form of log (Y) = 0.1714 log (X) + 1.4476 (Fig. 5B). The LoD was estimated to 0.23 nM using the equation LoD = 3σ/s [39,49]. The σ was the relative standard deviation of the fluorescence intensity of the blank control and s was the slope of the calibration curve. The LoD was lower than that of previously reported carbon nanobelts (5 nM) [50], Cu(H_2dtoa) MOFs (3 nM) [51], zwitterionic zinc(II)-carboxylate polymers (7.4 nM) [52], zinc-methylimidazolate framework-8 (1.2 nM) [53] for HIV detection and comparable to that of recently reported [Cu(Dcbcp)(bpe)]n (0.2 nM) [54] for ZIKV RNA assay. In Table 1, we show that the performance of the NPC is comparably or even favorably to other nanomaterials, in terms of the LoD and the quantification range.

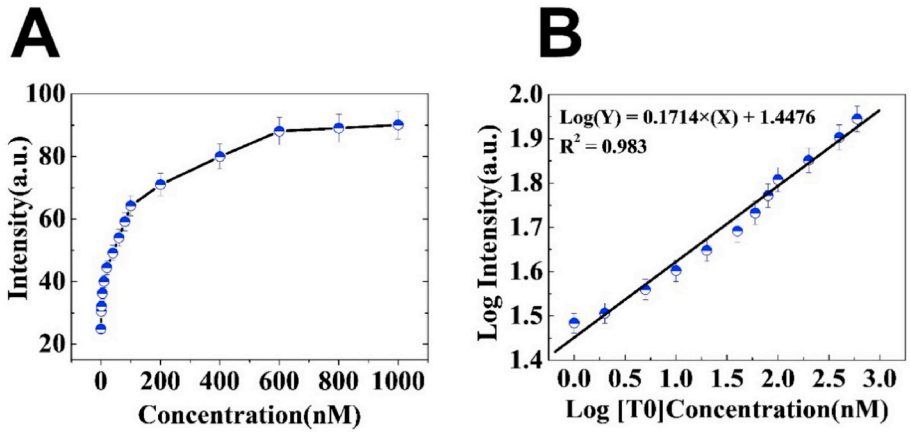

Fig. 5. (A) Fluorescent intensity of P-DNA@NPC complex after incubating with different concentrations of T-RNA (0, 1, 2, 5, 10, 20, 40, 60, 80, 100, 200, 400, 600, 800, 1000 nM); (B) The linear calibration plots of fluorescent intensity of P-DNA against T-DNA concentrations.

3.6. Selectivity analysis

In addition to sensitivity, the selectivity towards specific target molecules is also an important parameter when evaluating the performance of a sensing system. In this study, complementary T-RNA (T0) and three kind of the mutation sequences including single-base mismatched T-RNA (T1), double-base mismatched T-RNA (T2) and non-complementary T-RNA (T3) at a fixed concentration (600 nM) were used to investigate the selectivity of the NPC and the possibility of detecting mutations. As shown in Fig. 6A, the fluorescence image of T1 is significantly darker than the T0. The image brightness of T2 or T3 is almost identical to the signal of the Tris-HCl buffer solution. As shown in Fig. 6B, the RE of T1 (92%) is significantly less than the value obtained with T0 (245%). Also, almost no difference in fluorescence intensity was observed when the P-DNA@NPC system was exposed to the T2 or T3. These results primarily demonstrate that the P-DNA@NPC system is highly selective for correct T-RNA, as demonstrated by the smaller fluorescence recovery observed, even when testing oligonucleotide sequences with only single-base mismatch.

3.7. Storage stability and reusability analysis

Both NPC and P-DNA can be pre-stored in the PCR tubes for later use as needed. In fact, we in this work have performed the assays using the NPC several weeks beforehand. As for the P-DNA, the data shown in Fig. S5 confirm that, if maintained at 4 °C, the P-DNA retains its fluorescence even after 10 days of storage. For each new experiment, NPC was directly placed to interact with P-DNA in PCR tubes to form P-DNA@NPC sensor. Then, P-DNA@NPC complex was incubated with T-RNA to perform the assay.

In addition, the reuse properties of the NPC were also demonstrated.

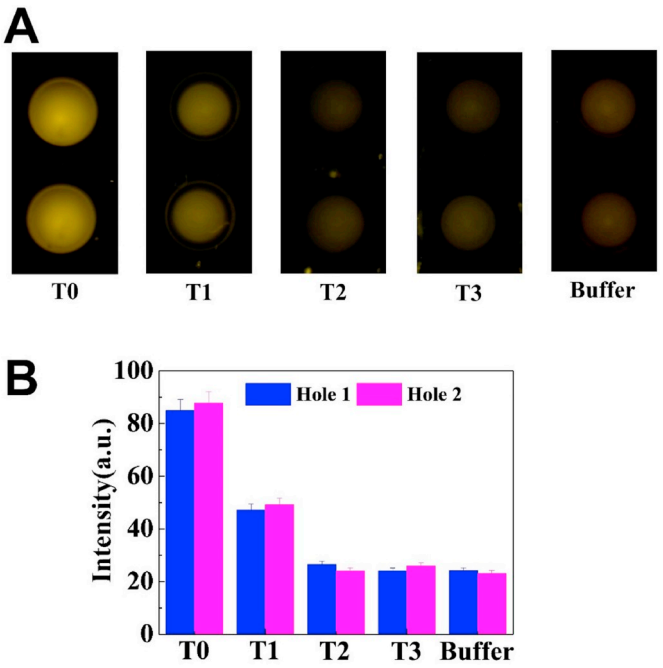

Fig. 6. Sensitivity analysis of P-DNA@NPC system for the discrimination. (A) Fluorescence recovery images by adding the different T-RNA: complementary T-RNA (T0), one-base mismatched T-RNA (T1), double-base mismatched T-RNA (T1), non-complementary T-RNA (T3), and Tris-HCl buffer solution; (B) Fluorescence intensity by adding the different T-RNA. The concentration of T-RNA is 600 nM.

Table 1
A comparison of various nanomaterials-based nucleic acid sensors.

Materail	Target	Linear range	Real sample matrix tested	Limit of detection	Ref
Carbon nanobelts (CNBs)	HIV	5–300 nM	No	5 nM	[50]
Poly(p-phenylenediamine) nanobelt	HIV	30–300 nM	No	30 nM	[58]
Single-walled carbon nanohorn	HIV	0–300 nM	No	1 nM	[59]
PPY nanospheres	HIV	1–300 nM	No	1 nM	[16]
zinc-methylimidazolate framework-8(ZIF-8)	HIV	10–100 nM	No	1.2 nM	[53]
Cu(H2dtoa) MOFs	HIV	10–100 nM	No	3 nM	[51]
Zwitterionic zinc(II)-carboxylate polymers	HIV	0–60 nM	No	7.4 nM	[52]
[Cu(Dcbcp)(bpe)]n	ZIKV	0.5–70 nM	No	0.2 nM	[54]
[Cu(Dcbb)(bipy)(OH)]n	ZIKV	0–50 nM	No	0.2 nM	[60]
Polypyrrole (PPY) film	–	–	Human blood serum	1.1 nM	[39]
Magnetic porous carbon (MPC)	HIV	0–600	Fetal bovine serum	1 nM	[25]
Nitrogen-doped porous carbon	ZIKV	0–600	Saliva sample	0.23 nM	This work

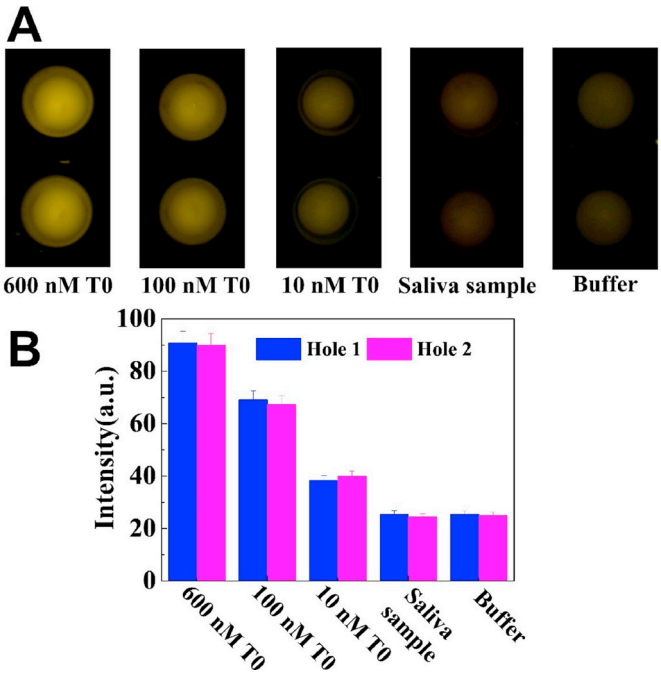

Fig. 7. Selectivity of P-DNA@NPC system for the discrimination of T-RNA in complex samples. (A) Fluorescence recovery images by adding the different T-RNA: 600 nM, 100 nM, 10 nM T-RNA spiked in saliva samples, saliva samples and Tris-HCl buffer solution; (B) Fluorescence intensity by adding the different T-RNA.

This experiment was repeated for five times. Interestingly, the recycled NPC still showed quenching ability to P-DNA. Then, P-DNA@NPC complex was incubated with T-RNA to perform the assay. Detailed information about the recycling methods of the NPC are shown in the Supplementary Material. Table S1 shows the results of the recycled NPC for the detection of 600 nM ZIKV RNA sequences in Tris-HCl buffer solution. The RE is about 255% and the relative standard deviations (RSD, n = 5) are around 4.9%. These results suggest that the NPC@P-DNA proposed here allows simple quantitative evaluation of ZIKV RNA sequences and provides a new perspective for the application of porous carbons in the field of fluorescence biomolecular sensing.

3.8. Analyze in complex samples

Previous researches have shown that the ZIKV existed in human saliva [55–57]. To assess the application potential of P-DNA@NPC system in analyzing actual samples, we tested its performance for detecting the T-RNA spiked in saliva samples. The fluorescent sensing assays were carried out under the optimized conditions described in Section 3.4. The fluorescence intensity of the P-DNA@NPC in the presence of saliva sample is almost identical to the signal of the Tris-HCl buffer solution (Fig. 7A). In addition, it can be seen that 600 nM T-RNA shows much higher fluorescence intensity than any of 100 nM and 10 nM T-RNA, diluted saliva samples, and Tris-HCl buffer solution. Specifically, the introduction of 600 nM T-RNA resulted in significant fluorescence enhancement with RE value being 258%. Under the same conditions, the RE was 171% for 100 nM T-RNA, and 56% for 10 nM T-RNA, respectively (Fig. 7B). The results were indicative that the NPC showed excellent potential for the ZIKV RNA sequences assay in the real samples and also had an attractive possibility for future diagnosis application. However, several challenges must be faced before a direct application of the NPC for the analysis of real patient samples. For example, how to convert the dsDNA existed in the complex biological samples to ssDNA required by the NPC remains a problem need to address in this field.

4. Conclusion

In this work, NPC was successfully synthesized in a simply and inexpensively model, and used for the selective fluorescence detection of ZIKV RNA sequences with a CCD-based imaging platform. The results indicated that NPC exhibited high sensitivity, with a LoD of 0.23 nM. It was demonstrated that the intensity of the recovery fluorescence was linear when the concentrations of the ZIKV T-RNA were varied from 1 to 600 nM. In addition, it was found that NPC was highly selective and can even distinguish the completely complementary sequences and those with only a base mismatch. Moreover, NPC was effective at detecting ZIKV RNA sequences in the complex cultures such as human saliva samples. Our advantage comes from the use of inexpensive NPC, the alleviation of laborious preparation, as well as the facile direct detection procedures which is critical for further analysis of infectious disease. Thus, this highly selective and sensitive biosensor might be available for the practical application in future. In addition, these findings in this paper could provide reference for the synthesis of more MOFs-derived porous carbons with potential applications in the early diagnosis of infectious diseases. In addition, the strategy proposed in this paper is also universal for early diagnosis of other infectious viruses. We are currently exploring MOFs-derived porous carbon for the early diagnosis of various epidemic diseases, such as Ebola, Dengue, Chikungunya, and others with similar clinical manifestations and geographical distributions.

Statement of conflicts

The authors declare no competing financial interest.

Acknowledgments

This work was financially supported by the National Natural Science Foundation of China (31800713 and 21806001); Dean's Fund of Hefei Institute of Physical Science, China (YZJJ2018QN22). Jie Li and Ke Yang thank Dr. lin from University of Manitoba for his kind suggestion.

Appendix A. Supplementary data

Supplementary data to this article can be found online at https://doi.org/10.1016/j.talanta.2019.06.091.

References

[1] P.P. Garcez, E.C. Loiola, R.M.D. Costa, L.M. Higa, P. Trindade, R. Delvecchio, J.M. Nascimento, R. Brindeiro, A. Tanuri, S.K. Rehen, Zika virus impairs growth in human neurospheres and brain organoids, Science 352 (6287) (2016) 816–818.
[2] F.R. Cugola, I.R. Fernandes, F.B. Russo, B.C. Freitas, J.L. Dias, K.P. Guimarães, C. Benazzato, N. Almeida, G.C. Pignatari, S. Romero, The Brazilian Zika virus strain causes birth defects in experimental models, Nature 534 (7606) (2016) 267–271.
[3] V.M. Cao-Lormeau, C. Roche, A. Teissier, E. Robin, A.L. Berry, H.P. Mallet, A.A. Sall, D. Musso, Zika virus, French polynesia, South Pacific, 2013, emerg, Inf. Disp. 20 (6) (2014) 1085–1086.
[4] T. Demir, S. Kilic, Zika virus: a new arboviral public health problem, Folia Microbiol. 61 (6) (2016) 523–527.
[5] J. Mlakar, M. Korva, N. Tul, M. Popović, M. Poljšakprijatelj, J. Mraz, M. Kolenc, K. Resman Rus, T. Vesnaver Vipotnik, V. Fabjan Vodušek, Zika virus associated with microcephaly, N. Engl. J. Med. 374 (10) (2016) 951–958.
[6] CDC, https://www.cdc.gov/zika/hc-providers/testing-guidance.html, (2019).
[7] O. Faye, O. Faye, D. Diallo, M. Diallo, M. Weidmann, A.A. Sall, Quantitative real-time PCR detection of Zika virus and evaluation with field-caught Mosquitoes, Virol. J. 10 (1) (2013) 311–318.
[8] M. Safavieh, M.K. Kanakasabapathy, F. Tarlan, M.U. Ahmed, M. Zourob, W. Asghar, H. Shafiee, Emerging loop-mediated isothermal amplification-based microchip and microdevice technologies for nucleic acid detection, ACS Biomater. Sci. Eng. 2 (3) (2016) 278–294.
[9] J. Song, M.G. Mauk, B.A. Hackett, S. Cherry, H.H. Bau, C. Liu, Instrument-free point-of-care molecular detectionof Zika virus, Anal. Chem. 88 (14) (2016) 7289–7294.
[10] C.J. Haug, M.P. Kieny, B. Murgue, The Zika challenge, N. Engl. J. Med. 374 (19) (2016) 1801–1803.
[11] D.J. Maxwell, J.R. Taylor, N. Shuming, Self-assembled nanoparticle probes for

recognition and detection of biomolecules, J. Am. Chem. Soc. 124 (32) (2002) 9606–9612.
[12] C. Zhu, Z. Zeng, H. Li, F. Li, C. Fan, H. Zhang, Single-layer MoS2-based nanoprobes for homogeneous detection of biomolecules, J. Am. Chem. Soc. 135 (16) (2013) 5998–6001.
[13] H. Li, J. Tian, W. Lei, Y. Zhang, X. Sun, Multi-walled carbon nanotubes as an effective fluorescent sensing platform for nucleic acid detection, J. Mater. Chem. 21 (3) (2010) 824–828.
[14] C.H. Lu, H.H. Yang, C.L. Zhu, X. Chen, G.N. Chen, A graphene platform for sensing biomolecules, Angew. Chem. 48 (26) (2010) 4785–4787.
[15] B. Liu, J. Liu, DNA adsorption by magnetic iron oxide nanoparticles and its application for arsenate detection, Chem. Commun. 50 (62) (2014) 8568–8570.
[16] W. Lu, Y. Luo, G. Chang, X. Qin, F. Liao, X. Sun, Polypyrrole colloidal nanospheres as an effective fluorescent sensing platform for DNA detection, Synthetic Met 161 (15–16) (2011) 1766–1770.
[17] L. Sen, W. Lei, L. Yonglan, T. Jingqi, L. Hailong, S. Xuping, Polyaniline nanofibres for fluorescent nucleic acid detection, Nanoscale 3 (3) (2011) 967–969.
[18] S. Dang, Q.L. Zhu, Q. Xu, Nanomaterials derived from metal–organic frameworks, Nat. Rev. Mater. 3 (2017) 17075.
[19] J. Li, X. Wang, G. Zhao, C. Chen, Z. Chai, A. Alsaedi, T. Hayat, X. Wang, Metal-organic framework-based materials: superior adsorbents for the capture of toxic and radioactive metal ions, Chem. Soc. Rev. 47 (7) (2018) 2322–2356.
[20] H.Q. Zhao, S.P. Yang, N.N. Ding, L. Qin, G.H. Qiu, J.X. Chen, W.H. Zhang, W.H. Chen, T.S. Hor, A zwitterionic 1D/2D polymer co-crystal and its polymorphic sub-components: a highly selective sensing platform for HIV ds-DNA sequences, Dalton Trans. 45 (12) (2016) 5092–5100.
[21] L. Qin, L.X. Lin, Z.P. Fang, S.P. Yang, G.H. Qiu, J.X. Chen, W.H. Chen, A water-stable metal-organic framework of a zwitterionic carboxylate with dysprosium: a sensing platform for Ebolavirus RNA sequences, Chem. Commun. 52 (1) (2015) 132–135.
[22] S.P. Yang, S.R. Chen, S.W. Liu, X.Y. Tang, L. Qin, G.H. Qiu, J.X. Chen, W.H. Chen, Platforms formed from a three-dimensional Cu-based zwitterionic metal-organic framework and probe ss-DNA: selective fluorescent biosensors for human immunodeficiency virus 1 ds-DNA and Sudan virus RNA sequences, Anal. Chem. 87 (24) (2015) 12206–12214.
[23] H.Q. Zhao, G.H. Qiu, Z. Liang, M.M. Li, B. Sun, L. Qin, S.P. Yang, W.H. Chen, J.X. Chen, A zinc(II)-based two-dimensional MOF for sensitive and selective sensing of HIV-1 ds-DNA sequences, Anal. Chim. Acta 922 (2016) 55–63.
[24] H.S. Wang, Metal–organic frameworks for biosensing and bioimaging applications, Coord. Chem. Rev. 349 (2017) 139–155.
[25] H. Tan, G. Tang, Z. Wang, L. Qian, G. Jie, S. Wu, Magnetic porous carbon nanocomposites derived from metal-organic frameworks as a sensing platform for DNA fluorescent detection, Anal. Chim. Acta 940 (2016) 136–142.
[26] J.W. Zhang, H.T. Zhang, Z.Y. Du, X.Q. Wang, S.H. Yu, H.L. Jiang, Water-stable metal–organic frameworks with intrinsic peroxidase-like catalytic activity as a colorimetric biosensing platform, Chem. Commun. 50 (9) (2014) 1092–1094.
[27] Z.Q. Bai, L.Y. Yuan, L. Zhu, Z.R. Liu, S.Q. Chu, L.R. Zheng, J. Zhang, Z.F. Chai, W.Q. Shi, Introduction of amino groups into acid-resistant MOFs for enhanced U(VI) sorption, J. Mater. Chem. A 3 (2) (2014) 525–534.
[28] W. Yang, X. Li, Y. Li, R. Zhu, H. Pang, Applications of metal–organic--framework-derived carbon materials, Adv. Mater. (2018) 1804740.
[29] Q. Duan, X. Li, Z. Wu, A. Alsaedi, T. Hayat, C. Chen, J. Li, Adsorption of 17β-estradiol from aqueous solutions by a novel hierarchically nitrogen-doped porous carbon, J. Colloid Interface Sci. 533 (2018) 700–708.
[30] I.A. Khan, Y. Qian, A. Badshah, M.A. Nadeem, D. Zhao, Highly porous carbon derived from MOF-5 as a support of ORR electrocatalysts for fuel cells, Acs Appl. Mater. Inter. 8 (27) (2016) 17268–17275.
[31] Y. Lin, C. Kong, Q. Zhang, L. Chen, Metal-organic frameworks for carbon dioxide capture and methane storage, Adv. Energy Mater. 7 (4) (2017) 1601296.
[32] X. Cao, C. Tan, M. Sindoro, H. Zhang, Hybrid micro-/nano-structures derived from metal–organic frameworks: preparation and applications in energy storage and conversion, Chem. Soc. Rev. 46 (10) (2017) 2660–2677.
[33] Z. Liu, B. Liu, J. Ding, J. Liu, Fluorescent sensors using DNA-functionalized graphene oxide, Anal. Bioanal. Chem. 406 (27) (2014) 6885–6902.
[34] C. Song, G.Y. Wang, D.M. Kong, A facile fluorescence method for versatile biomolecular detection based on pristine α-Fe2O3 nanoparticle-induced fluorescence quenching, Biosens. Bioelectron. 68 (2015) 239–244.
[35] H. Li, Y. Zhang, L. Wang, J. Tian, X. Sun, Nucleic acid detection using carbon nanoparticles as a fluorescent sensing platform, Chem. Commun. 47 (3) (2011) 961–963.
[36] G.P. Göertz, S.R. Abbo, J.J. Fros, G.P. Pijlman, Functional RNA during Zika virus infection, Virus Res. 254 (2017) 41–53.
[37] Z.B. Yu, Y.G. Hui, D.F. Lei, C.Y. Chin, V.R.C., S. Banumathi, K.C. Cheng, L.P. Wei, Structure and function of the Zika virus full-length NS5 protein, Nat. Commun. 8 (2017) 14762.
[38] Y.F. Wu, J.Y. Han, X. Peng, R. Xu, Y.J. Kang, Nano metal-organic framework (NMOF)-based strategies for multiplexed microRNA detection in solution and living cancer cells, Nanoscale 7 (5) (2014) 1753–1759.
[39] G.C. Pedro, F.D. Gorza, R.J. da Silva, K.T. do Nascimento, J.C. Medina-Llamas, A.E. Chávez-Guajardo, J.J. Alcaraz-Espinoza, C.P. de Melo, A novel nucleic acid fluorescent sensing platform based on nanostructured films of intrinsically conducting polymers, Anal. Chim. Acta 1047 (2018) 214–224.
[40] S.P. Yang, W. Zhao, P.P. Hu, K.Y. Wu, Z.H. Jiang, L.P. Bai, M.M. Li, J.X. Chen, Lanthanum-based metal–organic frameworks for specific detection of Sudan virus RNA conservative sequences down to single-base mismatch, Inorg. Chem. 56 (24) (2017) 14880–14887.
[41] G.H. Qiu, Z.H. Weng, P.P. Hu, W.J. Duan, B.P. Xie, B. Sun, X.Y. Tang, J.X. Chen, Synchronous detection of ebolavirus conserved RNA sequences and ebolavirus-encoded miRNA-like fragment based on a zwitterionic copper (II) metal–organic framework, Talanta 180 (2018) 396–402.
[42] Q. Zhang, C.F. Wang, Y.K. Lv, Luminescent switch sensors for the detection of biomolecules based on metal–organic frameworks, Analyst 143 (18) (2018) 4221–4229.
[43] S. Liu, H. Li, W. Lei, J. Tian, X. Sun, A new application of mesoporous carbon microparticles to nucleic acid detection, J. Mater. Chem. 21 (2) (2010) 339–341.
[44] H.S. Wang, H.L. Liu, K. Wang, Y. Ding, J.J. Xu, X.H. Xia, H.Y. Chen, Insight into the unique fluorescence quenching property of metal-organic frameworks upon DNA binding, Anal. Chem. 89 (21) (2017) 11366–11371.
[45] L. Hailong, Z. Yingwei, W. Lei, T. Jingqi, S. Xuping, Nucleic acid detection using carbon nanoparticles as a fluorescent sensing platform, Chem. Commun. 47 (3) (2010) 961–963.
[46] Y.Q. Wen, F.F. Xing, S.J. He, S.P. Song, L.H. Wang, Y.T. Long, L. Di, C.H. Fan, A graphene-based fluorescent nanoprobe for silver(I) ions detection by using graphene oxide and a silver-specific oligonucleotide, Chem Commun, Chem. Commun. 46 (15) (2010) 2596–2598.
[47] Y.H. Wang, H.H. Deng, Y.H. Liu, X.Q. Shi, A.L. Liu, H.P. Peng, G.L. Hong, W. Chen, Partially reduced graphene oxide as highly efficient DNA nanoprobe, Biosens, Bioelectron 80 (2016) 140–145.
[48] L.B. Zhang, T. Li, B.L. Li, J. Li, E. Wang, Carbon nanotube-DNA hybrid fluorescent sensor for sensitive and selective detection of mercury(II) ion, Chem. Commun. 46 (9) (2010) 1476–1478.
[49] Y.D. Ye, L. Xia, D.D. Xu, X.J. Xing, D.W. Pang, H.W. Tang, DNA-stabilized silver nanoclusters and carbon nanoparticles oxide: a sensitive platform for label-free fluorescence turn-on detection of HIV-DNA sequences, Biosens. Bioelectron. 85 (2016) 837–843.
[50] X. Sun, Z. Xing, R. Ning, A.M. Asiri, A.Y. Obaid, Carbon nanobelts as a novel sensing platform for fluorescence-enhanced DNA detection, Analyst 139 (10) (2014) 2318–2321.
[51] X. Zhu, H. Zheng, X. Wei, Z. Lin, L. Guo, B. Qiu, G. Chen, Metal–organic framework (MOF): a novel sensing platform for biomolecules, Chem. Commun. 49 (13) (2013) 1276–1278.
[52] B. Sun, H.Q. Zhao, B.P. Xie, L.P. Bai, Z.H. Jiang, J.X. Chen, Sequence-specific fluorometric recognition of HIV-1 ds-DNA with zwitterionic zinc(II)-carboxylate polymers, J. Inorg. Biochem. 176 (2017) 17–23.
[53] Y. Pan, S. Zhan, F. Xia, Zeolitic imidazolate framework-based biosensor for detection of HIV-1 DNA, Anal. Biochem. 546 (2018) 5–9.
[54] B.P. Xie, G.H. Qiu, P.P. Hu, Z. Liang, Y.M. Liang, B. Sun, L.P. Bai, Z.H. Jiang, J.X. Chen, Simultaneous detection of Dengue and Zika virus RNA sequences with a three-dimensional Cu-based zwitterionic metal–organic framework, comparison of single and synchronous fluorescence analysis, Sensor. Actuator. B Chem. 254 (2018) 1133–1140.
[55] C. Fourcade, J.-M. Mansuy, M. Dutertre, M. Delpech, B. Marchou, P. Delobel, J. Izopet, G. Martin-Blondel, Viral load kinetics of Zika virus in plasma, urine and saliva in a couple returning from Martinique, French West Indies, J. Clin. Virol. 82 (2016) 1–4.
[56] D. Musso, C. Roche, T.-X. Nhan, E. Robin, A. Teissier, V.-M. Cao-Lormeau, Detection of Zika virus in saliva, J. Clin. Virol. 68 (2015) 53–55.
[57] A.C. Gourinat, O. O'Connor, E. Calvez, C. Goarant, M. Dupont-Rouzeyrol, Detection of Zika virus in urine, Emerg. Infect. Dis. 21 (1) (2015) 84–86.
[58] W. Lei, Z. Yingwei, T. Jingqi, L. Hailong, S. Xuping, Conjugation polymer nanobelts: a novel fluorescent sensing platform for nucleic acid detection, Nucleic Acids Res. 39 (6) (2011) 1–6.
[59] S.Y. Zhu, Z.Y. Liu, W. Zhang, S. Han, L.Z. Hu, G.B. Xu, Nucleic acid detection using single-walled carbon nanohorns as a fluorescent sensing platform, Chem. Commun. 47 (21) (2011) 6099–6101.
[60] B.P. Xie, G.H. Qiu, B. Sun, Z.F. Yang, W.H. Zhang, J.X. Chen, Z.H. Jiang, Synchronous sensing of three conserved sequences of Zika virus using a DNAs@MOF hybrid: experimental and molecular simulation studies, Inorg. Chem. Front. (2019) 10.1039/C8QI01031E.